Applied Catalysis B: Environmental 303 (2022) 120880

Contents lists available at ScienceDirect

Applied Catalysis B: Environmental

journal homepage: www.elsevier.com/locate/apcatb

Fe, N-doped carbonaceous catalyst activating periodate for micropollutant removal: Significant role of electron transfer

Lei He [a], Chao Yang [a], Jie Ding [a], Mei-Yun Lu [a], Cheng-Xin Chen [a], Guang-Yuan Wang [a], Jun-Qiu Jiang [a], Lan Ding [b], Guo-Shuai Liu [c], Nan-Qi Ren [a], Shan-Shan Yang [a,*]

[a] State Key Laboratory of Urban Water Resource and Environment, School of Environment, Harbin Institute of Technology, Harbin 150090, China
[b] College of Chemistry, Jilin University, Changchun 130012, China
[c] School of Environmental and Civil Engineering, Jiangnan University, Wuxi 214122, China

ARTICLE INFO

Keywords:
Coagulation waste
Periodate
Electron transfer
DFT
Sulfadiazine

ABSTRACT

In this study, the performance of periodate (PI) on sulfadiazine (SDZ) degradation was evaluated using coagulation solid waste fabricated catalyst (CWBC), obtained by simple pyrolysis. SDZ effectively underwent 98.94% remove within 90 min in the CWBC/PI system. Electron transfer was the predominant mechanism due to the development of an electronic cycle among SDZ, CWBC and PI, where the $O_2^{\bullet-}$, PFRs, and the reactive iodine species had minor roles. Density functional theory calculations identified that Fe and N could change the electron configuration and break the chemical inertness of carbonaceous material. As a result, electrons on the carbon matrix of CWBC are inclined to travel through the formed Fe–O covalent bond to PI. Further analysis demonstrated that SO_4^{2-}, humic acid (HA), as well as anoxic conditions greatly facilitated SDZ degradation. This study provides a facile protocol for converting coagulation waste to an efficient catalyst and provides fundamental insights into the degradation mechanisms of micropollutants by activating PI.

1. Introduction

Due to increased environmental issues, advanced oxidation processes (AOPs) could be attractive options to mineralize viable refractory micropollutants [1]. These processes use strong oxidizing agents and produce powerful reactive species to attack persistent organic micropollutants. Among these oxidants, periodate (PI) has received increasing attention due to its stability, convenience for transportation and storage, and priorities when used in certain circumstances [2,3]. Compared to other oxidants, PI can be activated quickly to be used when the contaminants need to be removed urgently [2]. Also, the PI-dominated AOP process can be investigated as an alternative for some particular circumstances where other oxidants are not suitable. With the aid of bi-metallics [4,5], metallic compound [6], freezing [7], ultrasonication [8], alkali [9], and short wavelength UV irradiation [10–12], PI can be activated to generate high oxidizing species (reactive oxygen species (ROS) and reactive iodine species (RIS)) or through nonradical mechanism to destroy organic contaminants [13]. However, their applicability is limited by the excessive consumption of external energy and chemicals [14]. Therefore, it is necessary to develop more feasible and environmentally friendly catalysts to solve these problems.

Carbonaceous catalysts are frequently used as intriguing AOP catalysts to produce reactive redox species. They have several advantages, including resistance to acids and bases, tunable electronic structures, low cost, and high electrical conductivity [15]. Li et al. [16] investigated the activation of PI by granular activated carbon for dye degradation and showed that GAC could show interesting recycling properties, as 100% acid orange 7 (AO7) decolourization was maintained for over 10 cycles. Moreover, some investigations have demonstrated that doping of N, especially ones with incorporated transition metals (such as Fe and Co), to the carbon framework could change the electron configuration. In this way, it can reduce the chemical inertness of carbonaceous material, enhancing the electron transfer mechanism contributed nonradical pathway [17–21]. With localized unpaired electrons, N atoms doping is considered efficient in strengthening the catalytic performance of inert carbonaceous materials by adjusting the spin density and charge distribution [22,23]. Activation of IO_4^-, which is always associated with inter- or intramolecular electron transfer [4], was supposed to be promoted by a Fe, N co-doped carbonaceous catalyst. However, only a few studies have been conducted to investigate the activation of PI and the

* Corresponding author.
E-mail address: shanshanyang@hit.edu.cn (S.-S. Yang).

https://doi.org/10.1016/j.apcatb.2021.120880
Received 2 August 2021; Received in revised form 26 October 2021; Accepted 28 October 2021
Available online 1 November 2021

related mechanisms by carbon-based materials. In addition, fabricating co-doped carbonaceous materials are complicated and expensive, which is not practical for environmental application. Therefore, investigations on inexpensive precursors with transition metals and N for PI activation are necessary.

Production of pulp and paper pulp-based materials is one of the fastest-growing activities [24]. The coagulation step plays an essential role in the papermaking process and produces a high sludge volume [25,26]. After pyrolyzing at proper parameters, biochar prepared from pulp sludge was reported to be safe and meet the International Biochar Initiative (IBI) biochar classification criterion [27,28]. As a result, this study uses the inherent Fe, N, and lignocellulosic component in the coagulation waste (CW) to form Fe-, N-containing carbonaceous materials via direct pyrolysis.

Considering the aspects above, this study reports first time the activation of IO_4^- using CW-derived Fe, N co-doped catalyst, where no energy input is required. Considering that sulfonamides are among the essential synthetic antibiotics used in medicine and veterinary practice [29], this study used sulfadiazine (SDZ) as a model pollutant to test the reaction activity of the prepared catalyst-activated PI system. The objectives of this study were: (1) to evaluate the efficiency of CW activated PI system for SDZ decomposition; (2) to investigate the degradation kinetics and effects of various environmental factors; (3) to explore the main reactive species and catalytically active sites in PI activation for contaminant degradation; and (4) to discuss the degradation mechanism and reaction pathways of SDZ decomposition. Thus, this work could provide theoretical guidance for fabricating PI-activating catalysts and demonstrates that CW could be a promising candidate for heterogeneous catalysts of PI activation in wastewater treatment.

2. Materials and methods

2.1. Chemicals

SDZ, methanol (MeOH), humic acid (HA), fulvic acid, furfuryl alcohol (FFA), sulfamethoxazole (SMX), chlortetracycline hydrochloride (CTC), reactive red 2 (RR2), bisphenol A (BPA), ibuprofen (IBU), diclofenac (DCF), norfloxacin (NOR), deuterium oxide (D_2O), phenylhydrazine (PH), benzoic anhydride (BA), 2-bromo-1-phenylethanone (BrPE), PI, 5,5-dimethyl1-pyrroline N-oxide (DMPO, 97%), and 2,2,6,6-tetramethyl-4-piperidone (TEMP) were purchased from Sigma-Aldrich (Shanghai, China). P-benzoquinone (p-BQ) was purchased from Macklin (Shanghai, China). Deionized water (resistivity $\geq$ 18.2 MΩ cm^{-1}) was used to prepare the reagents and reaction solutions. Raw CW was provided by a paper mill in Heilongjiang Province, China, and stored at 4 °C to avoid biodegradation until further use.

2.2. Preparation of the catalyst

The collected material was oven-dried at 60 °C and then pyrolyzed in a vacuum tube furnace (Vacuum tube furnace, Shanghai Micro-X Furnace Co., Ltd., Shanghai, China) for 2 h at a heating temperature of 550 °C under oxygen-limited conditions. The as-obtained pyrolyzed material was treated by milling with an agate mortar and passing the milled powder through a 200-mesh sieve. The product was stored in dried glass vials for further use. The fabricated catalyst was named CWBC.

2.3. Experimental procedure

Unless otherwise specified, the degradation experiments were carried out in 250 mL beakers containing 100 mL of 40 μM SDZ solution and the desired initial dosage of 0.50 g L^{-1} CWBC catalyst at room temperature (25 ± 2 °C). The initial pH values of the SDZ solution were adjusted with 0.1 M NaOH or 0.1 M H_2SO_4 to a pH of 3 ± 0.05. 5 mM of PI was then added to the solution as a trigger for the degradation reaction. Magnetic stirring was applied at 400 RPM to ensure uniform dispersion of the CWBC catalyst.

At specific time intervals, 1 mL samples were withdrawn from the reaction system, immediately mixed with 1 mL sodium thiosulfate to terminate the reaction, and filtered through a 0.22 μm polyether sulfone filter (Millipore) for further analysis.

A recycling test was conducted for five cycles. After each cycle, the catalyst was separated from the reaction solution using suction filtration. Without recovering, the catalyst was dried in a drying oven at 60 °C for 12 h. The recycled catalyst was added into a new SDZ solution for the next catalytic cycle, and this was repeated five times.

Functional group deactivating experiments were conducted according to a previously reported method [5], by selectively deactivating ketonic carbonyl (C═O), hydroxyl (−OH) or carboxylic (−COOH) groups with PH, BA or BrPE, respectively. The CWBC derivatives prepared using PH, BA and BrPE are denoted CWBC-PH, CWBC-BA and CWBC-BrPE, respectively.

Quenching tests were conducted to identify ROS, determine electron transfer characteristics, and isolate their effects during SDZ degradation. Quenching was performed by adding excess MeOH, p-BQ, FFA, KI, and phenol to the solution before starting the reaction. All experiments were performed in triplicate for each condition.

2.4. Analysis

Morphological images of the samples were obtained by a scanning electron microscope (SEM) (Sigma 500, ZEISS, England) integrated with an energy-dispersive X-ray spectrometer (EDS) (X-MaxN, Oxford, England) and a high-resolution transmission electron microscopy (HR-TEM) (Tecnai F20, FEI Co., Hillsboro, OR, USA). The crystal structure was identified by a powder X-ray diffractometer (XRD) (Empyrean, Panalytical, Netherlands). X-ray photoelectron spectroscopy (XPS) was conducted to identify the variation of surface elemental valance states (K-alpha, Thermo Scientific, USA). Fourier transform infrared spectroscopy (FT-IR) (Nicolet 10, Thermo Scientific, USA) was used to characterize the major functional groups within the 400–4000 cm^{-1} range. The electron paramagnetic resonance (EPR) spectra were collected using a Bruker A300 spectrometer (EPR, Bruker Biospin GmbH, Rheinstetten, Germany) with 2,2,6,6-tetramethyl-4-piperidinol (TEMP) and 5,5-dimethyl-1-pyrroline N-oxide (DMPO) as the trapping agents. The dissolved Fe ions were quantified by plasma atomic emission spectrometry (ICP-OES) (5300DV PE Optima ICP-OES, USA). The total organic carbon (TOC) was determined by a TOC analyzer (TOC Analyzer, TOC-V_{CPH}, Shimadzu, Japan). The point of zero charges (pH_{pzc}) was recorded with a zeta voltmeter (ZP, Zetasizer Nano ZS90, Malvern, England).

SDZ was analyzed by a Waters ACQUITY ultra-performance liquid chromatography (UPLC, Waters, USA) equipped with a reverse-phase column (Waters, 50 mm × 2.1 mm, 1.7 μm) with a detection wavelength 265 nm. The detailed parameters are described in Text S1. IO_4^-, IO_3^- and I^- were analyzed using UPLC-MS/MS (UPLC-MS/MS, Open Architecture UPLC, Xevo TQ MS, Waters, USA) at the single ion recording (SIR) mode. The eluent composition is water and acetonitrile (65:35 v/v) with a flow rate of 0.3 mL min^{-1}. The column oven temperature was maintained at 35 ℃. The sample injection volume was 10 μL. IO_4^-, IO_3^- and I^- were analyzed under electrospray ionization source (ESI^-) with *m/z* of 190.88, 174.89, and 126.90, respectively. Quantification was performed by establishing the calibration curves using mixed standard solutions of $NaIO_4$, $NaIO_3$ and KI. The possible degradation intermediates of SDZ were identified by liquid chromatography/quadrupole time-of-flight mass spectrometry (QTOF LC/MS) (6545 QTOF LC/MS, Agilent, USA), under electrospray ionization source (ESI) between 50 *m/z* and 1000 *m/z*. The detailed parameters are described in Text S2.

Electrochemical measurements of CWBC were performed in a three-electrode cell (CHI 760E, CH Instrument, Shanghai) at 25 ± 2 °C. The

CWBC-loaded foam nickel electrode, Ag/AgCl electrode, and platinum wire were the working electrode, reference electrode, and counter electrode. The current-time curves (I-t curves) measurements were performed using 0.1 M Na_2SO_4 solution as the supporting electrolyte.

2.5. Theoretical calculations

First-principles calculations were performed using the density-functional-theory (DFT) in the "Vienna Ab initio Simulation Package" (VASP 5.4.1) with the detailed parameter settings in Text S3.

3. Results and discussion

3.1. Characterizations of CWBC

The surface morphology and microstructure of CWBC samples are revealed by SEM/HR-TEM micrographs and displayed in Fig. 1. Fluffily structured CWBC with a rough surface can be observed, with an average particle size of 10–20 μm (Fig. 1a). In the HRTEM micrographs, the CWBC catalyst exhibits an irregular multilayered structure with many spherical black particles uniformly dispersed in the carbon matrix (Fig. 1d–g). EDS elemental mappings of the CWBC samples shows that the five main elements of C, O, N, Fe and Si are distributed on the surface of CWBC throughout the entire architecture, indicating the co-doping of N and Fe in CWBC. Si, which is inactive in the AOP system, was originated from the papermaking process (Fig. 1b). These particles may be primarily iron or iron oxide. The calculated lattice distance of 0.221 nm of the black particles can be indexed as (113) of Fe_2O_3, demonstrating the existence of Fe oxides [30]. The HRTEM highlights the calculated crystalline lattice spacing of 0.337 nm, which fitted with the spacing of graphite layers (sp^2 hybridization) [31], indicating the existence of the graphitic carbon structures. From the XRD pattern (Fig. 2a), the broad reflection peak of CWBC reveals an amorphous structure. The only characteristic peak can be assigned to hexagonal graphite structure's (002) plane [14,32]. The sharp peaks are potentially relevant to the presence of inorganic phases such as Si, Na and Fe in the raw CWBC, consistent with the EDS mapping. Because of the small content of ≈ 1.9% identified by EDS on CWBC (Fig. 1c), no characteristic peaks of Fe were observed in the XRD pattern.

High-resolution XPS measurements were performed further to explore the surface chemical valence states of CWBC. In Fig. 2b, the bonding energies of fresh CWBC at 284.8 eV, 400.47 eV, 532.86 eV and 711.63 eV correspond to peaks of C 1s, N 1s, O 1s and Fe 2p, respectively. As seen in Fig. 2c, the deconvolution of the C 1s spectrum of fresh CWBC exhibits four peaks at 284.73 eV, 285.37 eV, 287.88 eV, and 290.24 eV, and these correspond to the C═C/C–C, C–O, C═O, and O–C═O groups, respectively. Fig. 2d presents the hyperfine XPS spectra of Fe. It shows the characteristic peaks at 711.35 eV and 723.19 eV, indexed to $Fe2p_{3/2}$ and $Fe2p_{1/2}$, respectively, with satellite peaks at 719.46 eV and 732.9 eV, which were attributed to Fe(III). The peaks centered at 714.97 eV and 728.1 eV are attributed to Fe(II) $2p_{1/2}$ of Fe (II) and its satellite peak, respectively [5]. The XPS Fe 2p spectra confirm the co-existence of the FeO and Fe_2O_3 phase in the CWBC catalyst. As reported, introducing N into the carbonaceous materials can contribute a pair of p-electrons to the graphitic carbon, increasing the activating ability [22]. Thereby, high-resolution XPS N 1s spectra were collected to quantify the types and contents of N dopants. As shown in Fig. 2e, the N 1s region can be deconvoluted into three peaks at binding energies of 398.29 eV, 400.48 eV, and 403.72 eV, which were respectively assigned to pyridinic N, pyrrolic N, and oxidized N [33].

3.2. Reaction activity and stability of the CWBC catalyst

A variety of control experiments were performed to evaluate in detail the SDZ removal performances. As displayed in Fig. 3a, SDZ was barely oxidized by PI without CWBC, as only 7.05% of SDZ was removed by PI within 90 min due to the low oxidation potential of IO_4^-. Thus, because of the low content of Fe leaching (Fig. S1), a homogeneous reaction

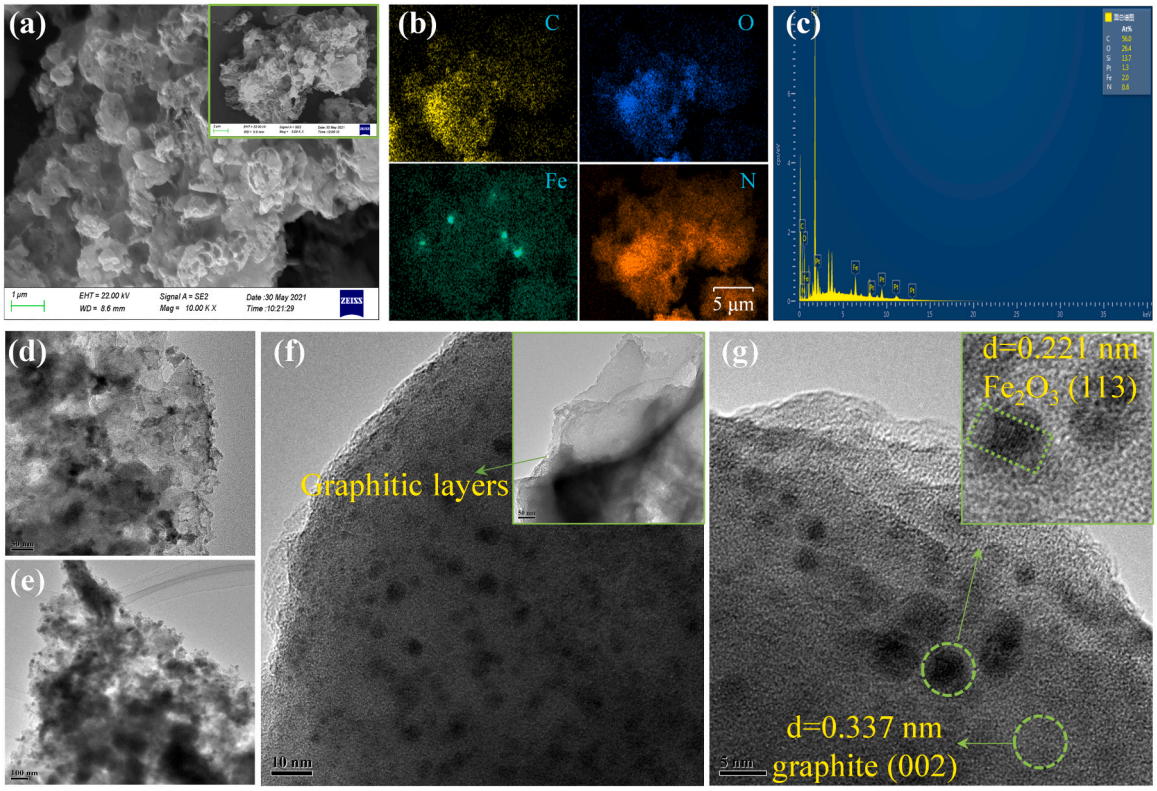

Fig. 1. (a) SEM micrographs, (b) EDS elemental mappings, (c) EDS elemental content, (d–g) different-magnification HRTEM of CWBC catalyst.

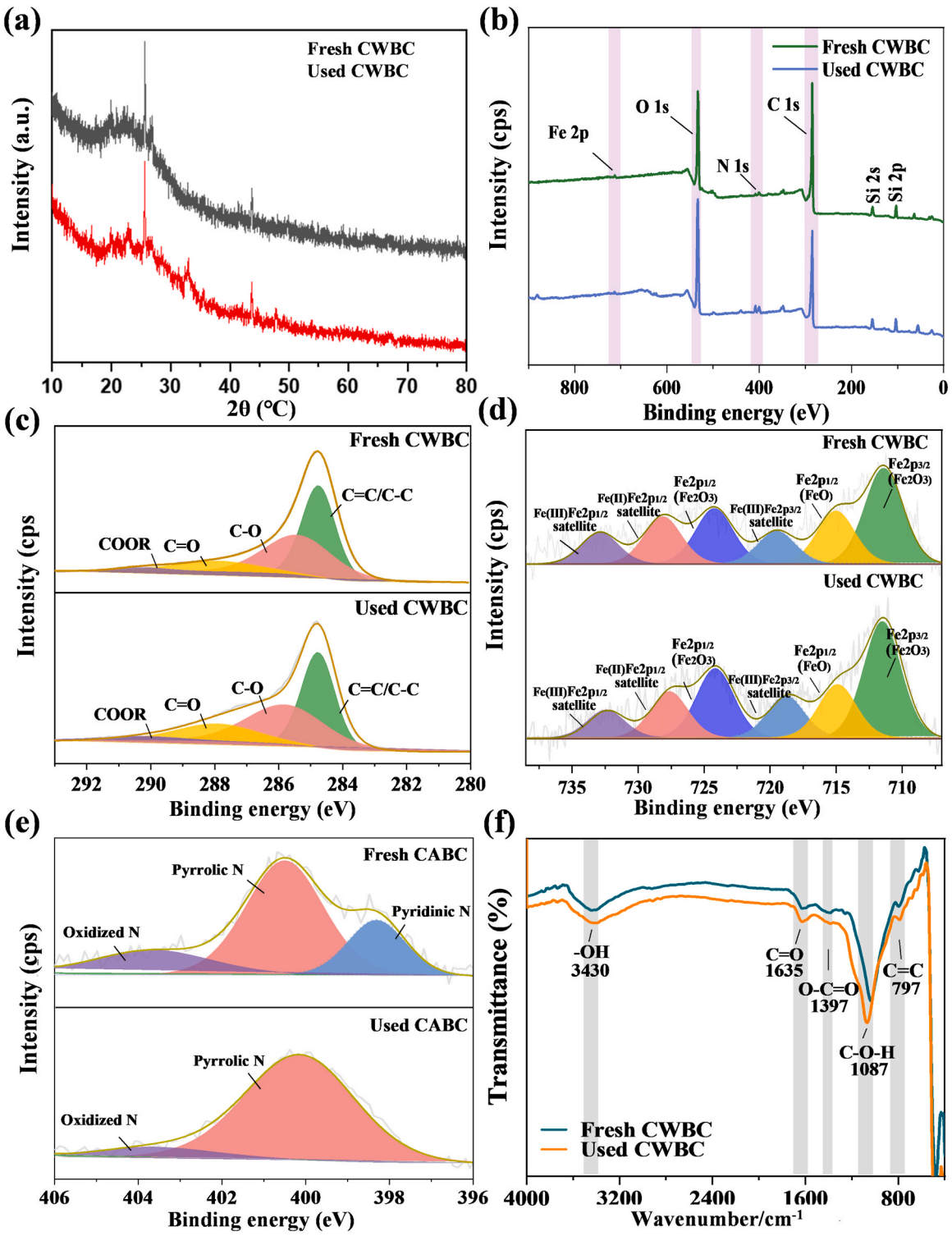

Fig. 2. (a) XRD pattern, (b) XPS survey scan spectra, (c) XPS C 1s spectra, (d) XPS Fe 2p spectra, (e) XPS N 1s spectra, (f) FT-IR of CWBC before and after reaction.

caused by Fe ions exerts a negligible effect (7.65%) on SDZ degradation, as ≈ 7% SDZ removal can be attributed to the PI oxidation. The use of CWBC without PI achieved 6.27% SDZ removal via adsorption within 90 min

In contrast, a high amount of SDZ (98.94%) was oxidized in the presence of both the CWBC catalyst and PI, reaching an aqueous TOC removal of ≈ 78% after 90 min of reaction. The calculated pseudo-first-order kinetic degradation rate (k_{obs}) was observed to increase remarkably to the value of 0.0586 min^{-1}. The excellent catalytic performance of the CWBC/PI system for SDZ degradation is supposed to be attributed to the following synergistic effects (1) the co-doping of N and Fe species can enhance the electron transfer mechanism for SDZ degradation; (2) Fe can promote the generation of persistent free radicals (PFRs) during pyrolyzing of biochar; (3) the transition metal ions could also activate the oxidizing agents. Detailed analysis will be discussed below.

Recycling experiments were conducted to test the stability and reusability of the CWBC catalyst (Fig. 3f). After five experimental cycles, the catalyst showed excellent stability, maintaining a removal rate of

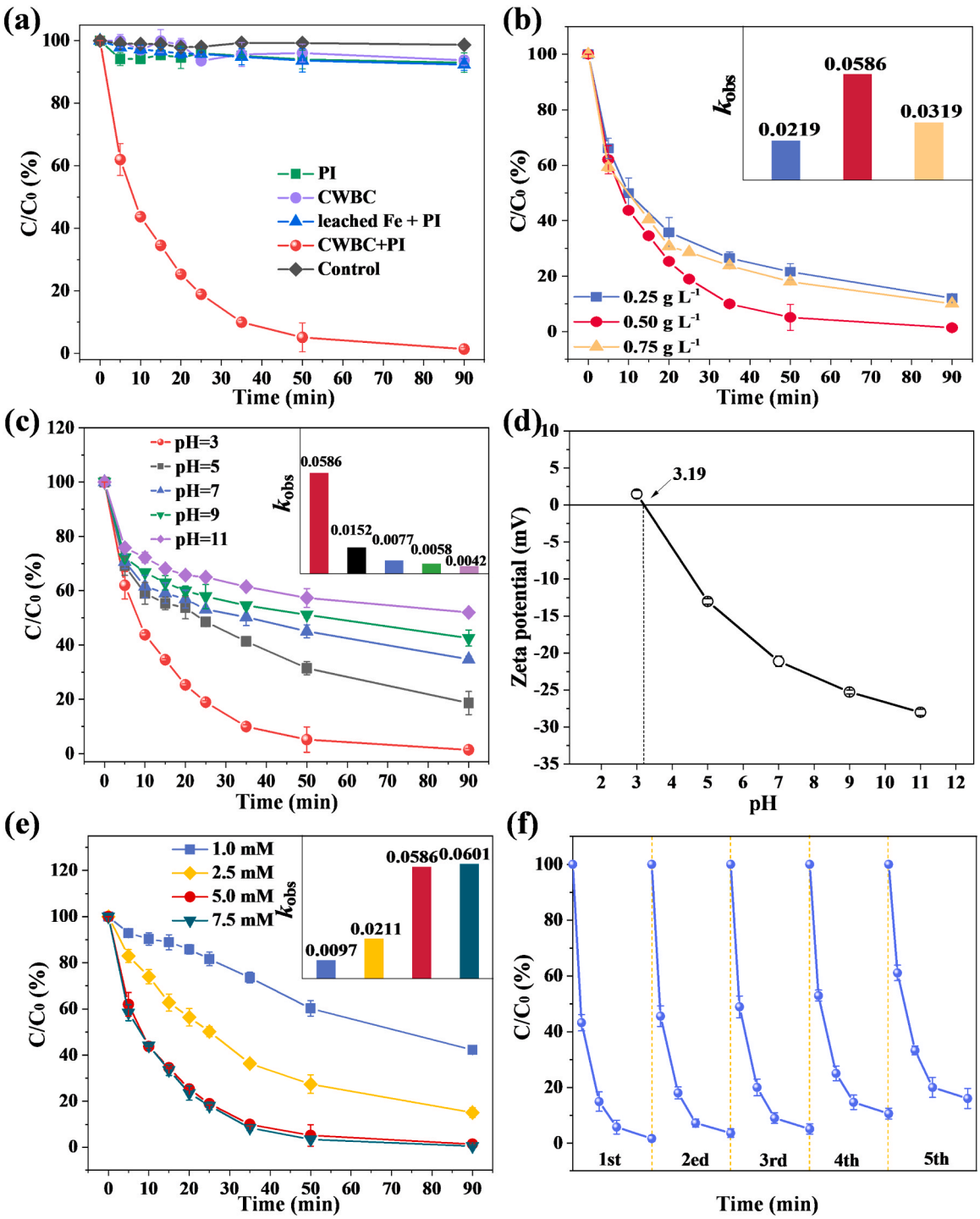

Fig. 3. (a) Removal of SDZ in various reaction system; effect of (b) CWBC catalyst dosage, (c) pH, (e) PI concentration on SDZ removal in CWBC/PI system (inset–first order rate constants for SDZ degradation in different reaction conditions); (d) zeta potential of CWBC at different pH value; (f) reusability of the CWBC for the SDZ removal. (Condition: $[SDZ]_0 = 40$ μM, CWBC catalyst dosage = 0.5 g L^{-1}, $[PI]_0 = 5.0$ mM, initial pH = 3.0).

> 80% of SDZ. Moreover, the morphologies and crystal structure of the CWBC catalyst showed no noticeable changes (characterized by XRD and SEM) (Fig. 2a and S2). From the FT-IR spectra and XPS C 1s spectrum (Fig. 2b–f), the small variations between fresh and used CWBC indicate possible participation of the functional groups in the reaction. Detailed verification of the contribution of the functional groups will be discussed in Section 3.5.4. Furthermore, the changes in characteristic peak areas of the Fe 2p spectrum before and after the catalytic process demonstrate the conversion of Fe species during the reaction (Fig. 2d). As shown in the XPS N 1s spectrum of the fresh and used CWBC (Fig. 2e), after usage, the intensity of pyridinic N reduced, implying that pyridinic N might serve as a reactive site. According to this study, two possible activation ways could exist: (i) following other reports, the existence of N breaks the symmetric distribution of the local electron cloud of pure carbonaceous material [34]. Pyridinic N with high electronegativity could reduce energy barrier and change the electron density of neighboring carbons during the catalytic reaction, withdrawing electrons from the adjacent carbons and then transferring to PI. Although N-doped

carbon material shows relatively weaker electron transfer with PI than the Fe, N co-doped material, the electron transfer effect still exists between N and PI. As a result, nitrogen configurations reconstruction could occur. Pyridinic N might be converted to oxidized N due to the electron transfer between N and PI. A similar phenomenon was also described by other references about the activation of persulfate (PS) by N-doped carbon nanotubes encapsulated with Fe nanoparticles [34] and about peroxydisulfate activation by nano-graphite [35]. (ii) N might act as an adsorption site. A previous study has reported that pyridinic N with lone electron pair can offer abundantly accessible active sites for the adsorption of ions and oxygen molecules on the material [21]. Similarly, as analyzed by the DFT calculation results detailed below, the observed weak interaction of PI with N suggests a physical absorption of IO_4^- on N atoms.

Based on the degradation efficiencies obtained in this system, the SDZ degradation performance was further investigated with different catalysts (such as copper-iron bimetallic oxides, biochar, solid waste residue, siderite, and MoS_2-Fe(III)) and oxidants (PMS, peroxodisulfate, and H_2O_2) reported in literature studies (Table S1). The CWBC/PI system described herein shows comparable performance in SDZ removal to those reported in other studies. Considering the enormous amount of waste material generated by coagulation, the usage of CW as a catalyst for PI activation and micropollutant degradation is a possible win-win strategy for waste disposal and contaminant removal.

3.3. Effect of reaction parameters on SDZ removal

The degradation of SDZ with the CWBC/PI system at pH 3 was evaluated by adding different concentrations of CWBC (0.25, 0.5, and 0.75 g L^{-1}, Fig. 3b). The degradation efficiency of SDZ improved, with corresponding pseudo-first-order rate constants (k_{obs}) of 0.0219 min^{-1} and 0.0586 min^{-1}, respectively, when the catalyst dosage increased from 0.25 to 0.50 g L^{-1}. However, the reaction k_{obs} decreased to 0.0319 min^{-1} when the amount of catalyst was increased to 0.75 g L^{-1}. Two reasons could explain this phenomenon. First, a higher dosage of catalyst brings excessive Fe(II), which would have a scavenging effect on active radicals generated in the solution with PI decomposition. Similar results have been found in the PS activation by sulfidated iron-nickel supported on biochar (S-FeNi@BC) catalysts [36] and nano zero-valent iron anchored yCo_3O_4 (nZVI/yCo_3O_4) composites [37]. Their main conclusion was that excessive Fe(II) could scavenge $SO_4^{\bullet-}$. Second, this phenomenon could be explained by the PI concentration limitation, which follows previous reports [38]. Thus, the optimal dosage of 0.5 g L^{-1} CWBC was maintained in this study.

Initial pH value is a vital factor that affects catalytic performance. In this study, SDZ degradation was favored in acidic and near-neutral pH conditions, reaching a peak removal rate (98.94% removal within 90 min) at pH 3.0 (Fig. 3c). Fig. 3d suggests that the pH_{pzc} value of CWBC is between 3.0 and 5.0. The positive zeta potential value around pH 3.0 indicates that a low pH value decreases the electrostatic repulsion between IO_4^- anions and the positively charged surface of the catalyst. As a result, CWBC can easily activate PI due to its favorable electrostatic forces on PI at pH 3. This activation is likely to appear due to the observed pH dependence of SDZ removal. On the contrary, the surface of CWBC is negatively charged when $pH > pH_{pzc}$, because of the dropped zeta potential of CWBC. This indicates that the increased pH caused electrostatic repulsion between the CWBC and PI, resulting in inhibition of SDZ degradation. Moreover, as the reported concentration-pH profile of the I^{VII} species show, I^{VII} species vary at different pH condition values [39]. The IO_4^- species are predominant at pH values below 8.0, while its dimerized form ($H_3IO_6^{2-}$) is dominant when the pH reaches 8.0 (Eqs. 1 and 2) [11,33]. Compared with the reduction potential of IO_4^-/IO_3^- (1.298 V), the value of $H_3IO_6^{2-}/IO_3^-$ (0.686 V) is lower, which is could be responsible for the relatively low degradation efficiency of SDZ at higher pH values.

$$H_5IO_6^- \leftrightarrow H_4IO_6^- + H^+, pka_1 = 1.64 \quad (1)$$

$$H_4IO_6^- \leftrightarrow H_3IO_6^{2-} + H^+, pka_1 = 8.36 \quad (2)$$

A positive correlation is observed between PI concentration and SDZ removal (Fig. 3e). A higher concentration of PI might produce more reactive compounds, which can result in a quicker degradation rate (from 0.0097 min^{-1} to 0.0586 min^{-1}), with the PI concentration increased from 1.0 mM to 5.0 mM. However, with an increase of PI concentration from 5.0 mM to 7.5 mM, the value of k_{obs} remained quasi-unchanged (from 0.0586 to 0.0601 min^{-1}), while the final removal efficiency was also not changed significantly. This finding is consistent with a study performed by Li et al. [16], who investigated AO7 degradation by PI-activated granular activated carbon. This phenomenon can potentially be explained by following aspects: first, excessive PI can compete for reactive radicals with SDZ (Eq. (3)); second, an excessive amount of CWBC is present when the PI concentration is lower than 5.0 mM. However, with the further addition of PI (above 5 mM), the higher concentration of PI cannot be activated entirely due to the limitation of CWBC dosage limitation [16].

$$IO_4^- + IO_3^{\bullet} \rightarrow IO_3^- + IO_4^{\bullet} \quad (3)$$

3.4. Effect of coexisting compounds on the CWBC/PI system

Ubiquitous water anions including nitrate (NO_3^-), chloride (Cl^-), bicarbonate (HCO_3^-) and sulfate (SO_4^{2-}) as well as dissolved organic matter (i.e., humic acid (HA)) are common influential factors in AOPs. Therefore, the efficiency of SDZ degradation was investigated of different coexisting matters with different concentrations. As H_2SO_4 was used as the pH-adjusting reagent in this study, SO_4^{2-} was first examined without adjusting the initial pH to determine the influence of H_2SO_4 addition to the reaction system (Fig. 4a and the corresponding reaction rate constant listed in Table S2). It can be mainly concluded that low concentrations (0.5–5 mM) of SO_4^{2-} exert an insignificant effect on SDZ degradation. However, at higher concentrations, a stronger inhibitory effect is visible. These results suggest that H_2SO_4, as a pH-adjusting agent, produces a negligible effect on the reaction system because less than 5 mM of SO_4^{2-} exists in the solution after adjusting the pH to 3 ± 0.5. A previous study also observed the same phenomenon [40], where SO_4^{2-} removed the Fe oxides on the CWBC surface, resulting in the increasingly release of Fe^{2+} and triggering the homogeneous reaction. A homogeneous reaction is generally regarded to own a higher reaction rate constant than a heterogeneous reaction [5].

After excluding the interference caused by SO_4^{2-}, the effect of other coexisting matters (except HCO_3^-, which shows a buffering capacity to change in pH) was investigated at pH 3. As shown in Fig. 4b and c and Table S2, Cl^- and NO_3^- exhibit a concentration-dependent inhibition on the removal of SDZ. The role of Cl^- on transition metals and AOPs involves complicated mechanisms and has shown controversial results [41]. No noticeable change in SDZ degradation was observed with low concentrations of Cl^-, with reaction rate constants of 0.0553 and 0.0455 min^{-1} (at Cl^- concentrations of 0.5 and 5 mM, respectively). However, when the concentration increased to 50–500 mM, an inhibitory effect on SDZ degradation was observed (k_{obs} = 0.0192 and 0.0118 min^{-1} for 50 and 500 mM, respectively). One hypothesis involves the inhibition effect by the high concentration of Cl^-, which probably forms an inorganic layer on the catalyst's surface, partially blocking the active sites [42]. A similar circumstance was found in a photocatalytic reaction with TiO_2 as the catalyst. Various salts can form an inorganic layer on the TiO_2 surface, inhibiting the adsorption of the contaminants on TiO_2 and decreasing its degradation capacity. Furthermore, Cl^- can scavenge reactive species to generate reactive chlorine species ($Cl^{\bullet}$ and $Cl_2^{\bullet-}$) and free chlorines (Cl_2 and HOCl). With the Cl^- concentration increase, less reactive $Cl_2^{\bullet-}$, Cl_2 and HOCl might form, lowering the oxidizing capacity of PI activated CWBC and

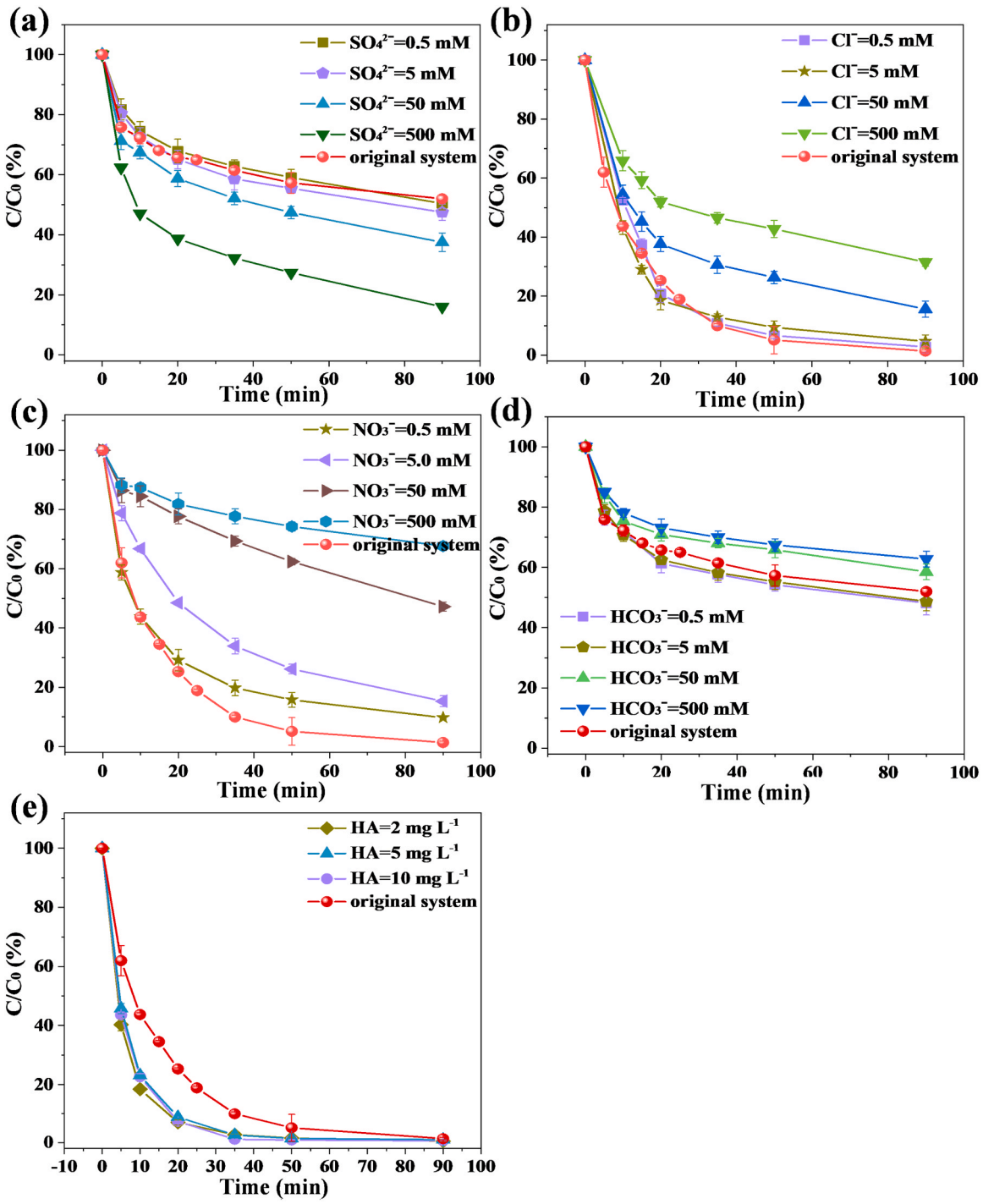

Fig. 4. Effect of different co-existed substances on SDZ degradation in the PI activated by CWBC: (a) SO_4^{2-}; (b) Cl^-; (c) NO_3^-; (d) HCO_3^-; (e) HA. (Reaction conditions: $[SDZ]_0 = 40$ μM, $[PI]_0 = 5.0$ mM, [CWBC] = 0.5 g L^{-1}, initial pH = 3.0).

reducing the efficiencies of SDZ degradation. Therein, $Cl_2^{\bullet-}$ is derived from the reaction between Cl^- and $IO_3^\bullet$ (Eqs (4) and (5)) [17]. Cl_2 and HOCl, which are particularly dominated at acidic conditions, are produced through self-quenching (Eqs. (6)–(9)) [43]. NO_3^- had a more significant inhibitory effect on SDZ degradation than Cl^-. This inhibition could be due to the quenching of ROS by NO_3^-, which consumes ROS species and produces less active substances ($NO_3^\bullet$) in the reaction system [17].

$$IO_3^\bullet + Cl^- \rightarrow IO_3^- + Cl^\bullet \quad (4)$$

$$Cl^\bullet + Cl^- \rightarrow Cl_2^{\bullet-} \quad (5)$$

$$Cl^\bullet + Cl^\bullet \rightarrow Cl_2 \quad (6)$$

$$Cl_2^{\bullet-} + Cl_2^{\bullet-} \rightarrow Cl_2 + 2Cl^- \quad (7)$$

$$Cl_2^{\bullet-} + Cl^\bullet \rightarrow Cl_2 + Cl^- \quad (8)$$

$$Cl_2 + H_2O \rightarrow HClO + H^+ + Cl^- \quad (9)$$

HCO_3^- can transform to H_2CO_3, HCO_3^-, and CO_3^{2-} with pH

variation due to its buffering capacity (Eqs. (10) and (11)). Thus, the initial pH was not adjusted when experiments were performed to investigate the influence of HCO_3^- on SDZ degradation of HCO_3^- [6]. The pH of the reaction system was approximately 11 without adjusting, causing the production of CO_3^{2-}. According to Fig. 4d, minor fluctuation could be observed when HCO_3^- concentrations varied from 0.5 to 5.0 mM. The unchanging removal rate could be attributed to the acceleration of Fe corrosion by HCO_3^-. In contrast, the catalytic efficiency slightly decreases with high concentrations of HCO_3^- (50–500 mM). There are two possible explanations for the inhibition of SDZ degradation with a high concentration of HCO_3^-: first, the generation of a passivation layer with Fe on CWBC particles, which can inhibit mass transfer, lowering the reactivity [44,45]. Second, CO_3^{2-} can act as a scavenger for reactive oxygen species ($k_{CO_3^{2-}+O_2^{\bullet-}} = 5.0 \times 10^8\ M^{-1}\ s^{-1}$) (Eqs. (12) and (13)) [6,46]. Similar findings were also reported in other studies: for instance, in the degradation of diclofenac sodium by PI activation, CO_3^{2-} was considered a highly effective hydroxyl scavenger [5]. The inhibition of the reaction by CO_3^{2-} manifests the results of the $O_2^{\bullet-}$ quenching experiment [40].

$$H_2CO_3 \leftrightarrow H^+ + HCO_3^-, pka_1 = 6.38 \quad (10)$$

$$HCO_3^- \leftrightarrow H^+ + CO_3^{2-}, pka_1 = 10.38 \quad (11)$$

$$CO_3^{2-} + O_2^{\bullet-} \leftrightarrow CO_3^{\bullet-} + O_2^{2-} \quad (12)$$

$$CO_3^{\bullet-} + O_2^{\bullet-} \leftrightarrow CO_3^{2-} + O_2 \quad (13)$$

The effect of HA on SDZ degradation was also investigated in this study (Fig. 4e). Compared with the system without HA, nearly complete SDZ removal was achieved with a reduced reaction time of 35 min. During the reaction, HA can promote the degradation of organic pollutants because it can enhance the electron transfer efficiency and the oxidation process [47]. HA contains abundant functional groups, especially quinone, and has been confirmed as acting as a redox shuttle. Meunier et al. [48] found HA could be complex with Fe and reduce the redox potential between the cycling of Fe(III) and Fe(II), thus boosting Fe(III)/Fe(II) cycling. In this study, the enhanced cycling of Fe species could be beneficial to PI activation, affecting the degradation efficiency of organic contaminants. These results indicate the potential applicability for practical and real-world water conditions. Moreover, HA can be used as an effective quencher of ROS [49]. The enhancement of SDZ degradation in the CWBC/PI/HA system implies that ROS is not the predominant removal mechanism in this catalytic reaction. The electron transfer mechanism might be the predominant pathway for SDZ degradation, with a detailed analysis discussed below.

3.5. Mechanism insights into SDZ degradation and PI activation

3.5.1. Identification of mechanism in CWBC/PI system

Various reactive species (ROS (hydroxyl radicals ($^{\bullet}OH$), superoxide radicals ($O_2^{\bullet-}$), singlet oxygen ($^1O_2$)), RIS ($IO_3^{\bullet}$ and $IO_4^{\bullet}$) and electron transfer are generally recognized as possible oxidizing pathway in PI oxidation systems [29]. Except for $IO_3^{\bullet}$, which could not be detected previously, the other three species are well known to oxidize organic pollutants at high reaction rates and can be identified via radical quenching tests. Consequently, the effect of selective ROS scavengers on

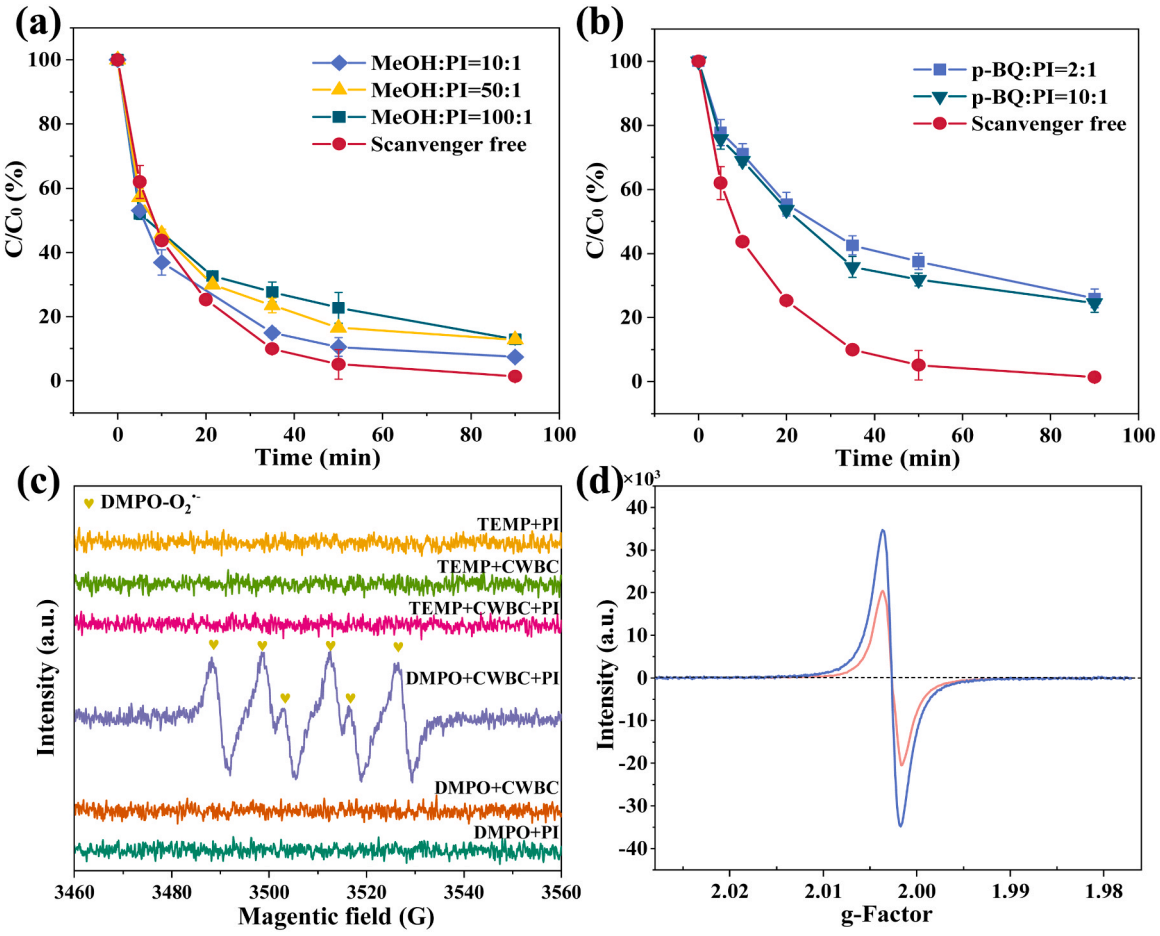

Fig. 5. Effect of quenching agents MeOH (a) and p-BQ (b) on the SDZ degradation in the PI activated by CWBC (Conditions: [SDZ] = 40 μM, catalyst dosage = 0.5 g L^{-1}, [PI] = 5.0 mM, initial pH = 3.0); EPR spectra of DMPO-$O_2^{\bullet-}$ (c) and PFRs (d).

SDZ oxidation was investigated in detail. The inhibitory effect of MeOH does not significantly impact the degradation of SDZ (Fig. 5a and Table S3), suggesting that the role of $^{\bullet}OH$ is negligible. 87.1% of SDZ is efficiently removed with a MeOH concentration as high as 500 mM. p-BQ was used as a scavenger for $O_2^{\bullet-}$ ($k_{O_2^{\bullet-}+p-BQ} = 1.0 \times 10^9\ M^{-1}\ s^{-1}$) [50]. About 25% of SDZ remove was suppressed with the addition of p-BQ, indicating the possible contribution of $O_2^{\bullet-}$ to SDZ degradation (Fig. 5b) (Eqs. (14)–(16)). Previous studies have proposed that $O_2^{\bullet-}$ can be produced in alkaline PI solutions (Eq. (16)) [9]. In this work, the optimal pH for SDZ degradation is ≈ 3, indicating that a small contribution to $O_2^{\bullet-}$ generation can be ascribed to the process detailed in Eq. (16). Therefore, heterogeneous Fe(II) is mainly involved in $O_2^{\bullet-}$ generation in this study (Eqs. (14) and (15)) [6]. This was also confirmed by XPS analysis confirming the conversion between Fe(II) and Fe(III) during the catalytic reaction (Fig. 2d). As the direct oxidation of $O_2^{\bullet-}$ to $^1O_2$ by residual PI is also a thermodynamically possible alternative pathway, the role of $^1O_2$ was tested by the convenient $^1O_2$ scavenger FFA ($k_{^1O_2+FFA} = 1.2 \times 10^8\ M^{-1}\ s^{-1}$) [51]. The results eliminated the possible contribution of $^1O_2$ oxygenation to SDZ degradation. Detailed analysis was discussed in the Supporting Information (Text S4, Fig. S3a).

$$Fe(II) + IO_4^- + H_2O \rightarrow Fe(III) + IO_3^- + O_2^{\bullet-} + 2H^+ \quad (14)$$

$$Fe(II) + O_2 \rightarrow Fe(III) + O_2^{\bullet-} \quad (15)$$

$$IO_4^- + 2OH^- \rightarrow 3IO_3^- + 2O_2^{\bullet-} + H_2O \quad (16)$$

EPR spectra of the reactive oxidizing species were monitored to provide additional evidence for the role of $^1O_2$ and $O_2^{\bullet-}$ on SDZ removal (Fig. 5c). No characteristic signal can be observed in the presence of TEMP/PI, TEMP/CWBC, DMPO/PI, or DMPO/CWBC, proving that there is almost no detectable ROS in these solutions. As expected, the characteristic signal of $^1O_2$ was not detected either, verifying the results of the H_2O and D_2O solvent exchange experiment (Fig. S3b). The particular spectrum (quartet signal, 1:1:1:1) can be observed, which is the characteristic signal of the DMPO-$O_2^{\bullet-}$ adduct. These results clearly demonstrate the existence of $O_2^{\bullet-}$ species during the catalytic process.

During low-temperature pyrolysis of biomass, the partially pyrolyzed products could complex with the existed transitional metals, forming PFRs, which can work as electron donors to transfer electrons to the inorganic oxidant used during the AOP, like PS [52]. Therefore, the detection of PFRs was conducted further to understand the electron transfer process in this reaction system. The results show that carbon-centered PFRs exist on the surface of CWBC, as recognized by the g-factor of 2.0027 [53] (Fig. 5d). After the catalytic reaction process, the decrease of the detected strong signal of PFRs implies the utilization of PFRs. Referring to the previous report that PS could be activated by single electron transfer from PFRs to PS to generate sulfate radicals, the carbon-centered PFRs are speculated to play a similar role of electron transfer [53]. With abundant unpaired electrons, PFRs can easily transport electrons to electron-deficient substances such as high valence transition metals. In the present study, the existence of Fe species meant that electrons could more likely transfer from PFRs to Fe species and then to PI, which is likely to be chemically adsorbed on Fe sites as discussed in 3.5.4 (Eqs. (17)–(20)). A similar phenomenon was previously been discussed by Wang et al. [54], who reported that PFRs in biochar could act as electron donors and accelerate the Fe(III)/Fe(II) cycle in the iron-based PS activation systems and results in the enhanced SMX removal rate.

$$Fe(II) \rightarrow Fe(III) + e^- \quad (17)$$

$$IO_4^- + 2H^+ + e^- \rightarrow IO_3^{\bullet} + H_2O \quad (18)$$

$$IO_4^- + IO_3^{\bullet} \rightarrow IO_4^{\bullet} + IO_3^- \quad (19)$$

$$IO_3^{\bullet} + SDZ \rightarrow IO_3^- + Products \quad (20)$$

3.5.2. Effect of dissolved oxygen on SDZ degradation in the CWBC/PI system

Because $O_2^{\bullet-}$ production is always associated with the existence of dissolved oxygen in the aqueous solution, the contribution of $O_2^{\bullet-}$ could be partially reflected by the changed atmosphere environment [30]. The reaction in our case was conducted in a deoxygenated solution with continuous nitrogen gas (N_2) purging to validate the role of dissolved oxygen. Unexpectedly, under these anoxic conditions, the SDZ degradation efficiency was significantly enhanced (Fig. 6a). More than 97.4% SDZ removal was achieved within 10 min under N_2 purging with excellent k_{obs} of 0.29 min^{-1}. This phenomenon shows that dissolved oxygen was dispensable for the degradation of SDZ by PI-activated CWBC [29].

To detect the origin of $O_2^{\bullet-}$ in this reaction system, p-BQ was used to verify the existence of $O_2^{\bullet-}$ under anoxic conditions (Fig. 6b). The results demonstrated that $O_2^{\bullet-}$ still exists and influences the degradation of SDZ under deoxygenated conditions, showing that O_2 is not essential for $O_2^{\bullet-}$ generation in this oxidative system. $O_2^{\bullet-}$ can be plausibly generated without O_2 participation, according to Eq. (14). Although the degradation rate decreases in the presence of p-BQ under these anoxic conditions, the reaction still achieves 86.25% degradation, but in this case, within 90 min. This phenomenon strongly indicates that other significant mechanisms could occur for SDZ removal in this reaction system.

Electron transfer is often responsible for the nonradical mechanism of carbon-based catalysts [46]. Electron transfer can facilitate the removal of organic compounds by transferring electrons from pollutants to PS with a carbonaceous catalyst as the electron shuttle [19,55]. Under oxidic conditions, dissolved oxygen can compete with IO_4^- to consume electrons, while competition does not occur under anoxic conditions. The promotion of SDZ degradation under anoxic conditions indicates that electron transfer might predominately contribute to the reaction process.

To verify this hypothesis, $K_2Cr_2O_7$, which is generally used to quench liquid-phase electrons to inhibit the possible generation of free radicals, was applied in this system (Fig. 6c) [56]. The efficiency of SDZ removal still achieves 65% in the presence of $K_2Cr_2O_7$, preliminarily showing that the surface reaction (following the electron transfer pathway) instead of radicals is the dominant mechanism responsible for SDZ degradation in the CWBC/PI system. Furthermore, because of the incomplete inhibitory effect of p-BQ (≈25%) and electron transfer (≈ 65%), RIS ($IO_3^{\bullet}$ and $IO_4^{\bullet}$) radicals as usually generated reactive species during the activation of PI only play an auxiliary role in the degradation of SDZ. The one-electron reduction of IO_4^- can produce the involvement of $IO_3^{\bullet}$ (Eqs. (17)–(20)) as discussed in Section 3.5.1, which is similar to the report by Lee et al. [4]. The radical pathway was not observed as a prominent mechanism during SDZ removal in the CWBC/PI system. This supports the hypothesis that electron transfer played the dominant role in SDZ degradation.

3.5.3. Role identification of electron transfer on SDZ degradation

To verify the effect of electron transfer on the reaction process, electrochemical measurements were carried out to monitor direct electron transfer over the surface of CWBC. A significant decrease in current was observed in the I-t curve upon the addition of PI (Fig. 6d), suggesting that the electron transfer happens between the CWBC electrode and PI. A decrease in current indicates that electrons transfer is mainly from the electrode to PI. The relatively high standard oxidation potential of PI ($E(IO_4^-/IO_3^-) = +1.60$ V vs NHE) caused it to act as the electron acceptor, which could pull out electrons from the catalyst by an electrostatic attraction [32]. This result shows that the electron transfer is generated by the transfer of electrons from CWBC to PI. The current density of the CWBC electrode significantly increases after the injection of SDZ, indicating that a surface reaction occurs. During this process, the degradation of SDZ is not caused by the electron transfer from PI, as

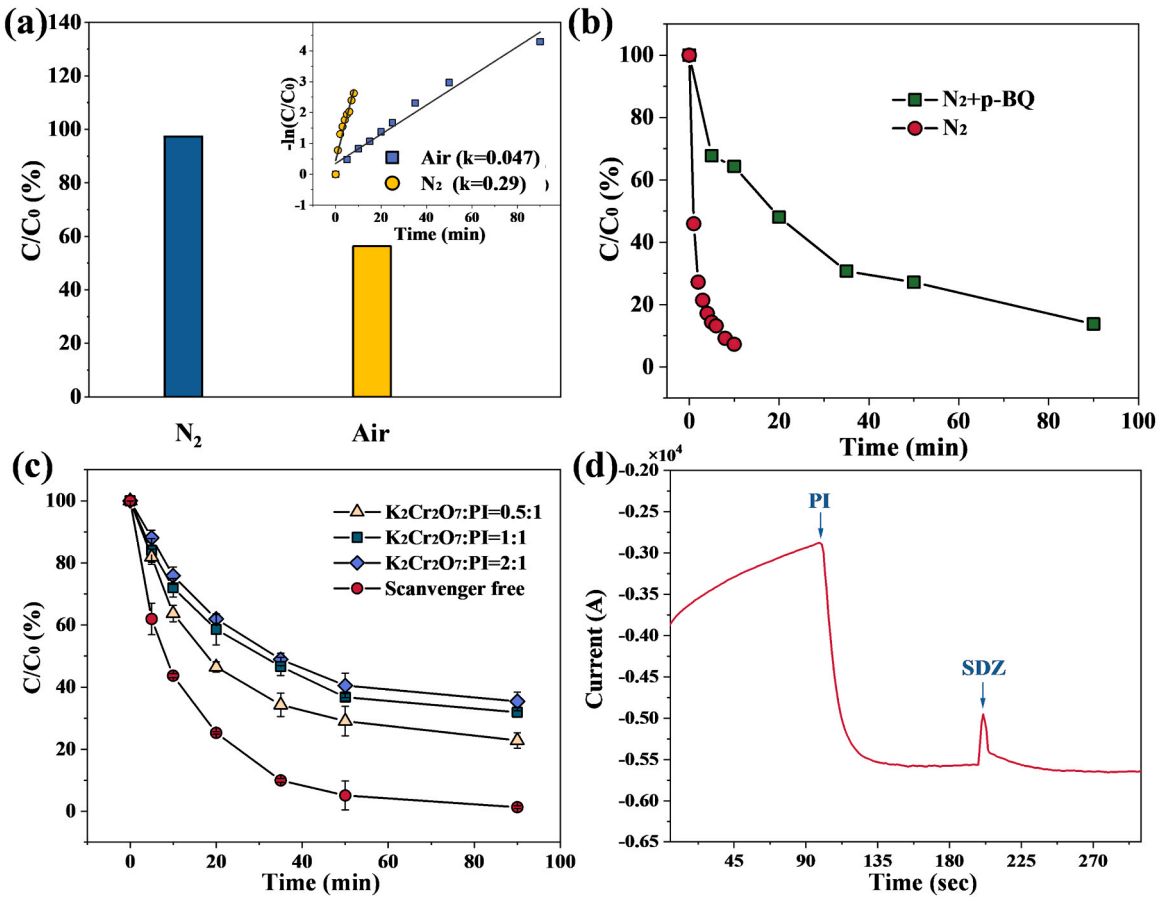

Fig. 6. (a) Influence of air on SDZ removal in CWBC/PI system (inset–first order rate constants for SDZ degradation under N_2 conditions); (b) Influence of p-BQ on SDZ removal under N_2 condition in CWBC/PI; (c) Influence of $K_2Cr_2O_7$ on SDZ removal under N_2 condition in CWBC/PI system; (d) I-t curves obtained at 0.0 V vs SHE (0.1 M Na_2SO_4) (Conditions: $[SDZ]_0$ = 40 μM, catalyst dosage = 0.5 g L^{-1}, $[PI]_0$ = 5.0 mM, initial pH = 3.0).

demonstrated by SDZ degradation, without the addition of CWBC (Fig. 3a), but caused by CWBC working as an electron shuttle. This is in line with previous reports, showing that electron transfer mediating a non-radical reaction pathway can be obtained by the conductive surface of carbonaceous materials [47].

3.5.4. *The inner mechanism of triggering electron transfer in the CWBC/PI activation system*

Surface functional groups including C−OH, −COOH and C═O can act as electron transfer mediators, promoting the generation of $IO_3^{\bullet}$. To assess the possible effect of these oxygen-containing functional groups on electron transfer in the reaction system, time profiles of SDZ removal by the derivatized functional groups of CWBC (CWBC-PH, CWBC-BA and CWBC-BrPE) as catalysts were performed (Fig. S4). The results reveal no noticeable change in SDZ degradation rate in the presence of the by the derivatized CWBC catalyst. Consistently, the FT-IR spectrum (Fig. 2f) displayed in 3.2 shows no significant change to the functional groups between raw and the used CWBC, manifesting a small effect of functional groups on SDZ degradation.

Based on the discussion above, radical (RIS and $O_2^{\bullet-}$) and non-radical (electron transfer) degradation processes take effect together for SDZ removal, wherein the electron transfer mechanism is dominant in the reaction process. The radicals derived from the IO_4^- and molecular oxygen activation by Fe(II) or PFRs (Eqs. (14) and (15) and (17)–(19)). Furthermore, the non-radical pathway referred to the CWBC-mediated electron transfer from SDZ to PI. In conclusion, the potential contribution of different mechanisms is proposed in order of electron transfer > ROS > RIS.

Theoretical calculations can provide an auxiliary effect on experimental data at the molecular and atomic levels and predict the rationality of the scheme theoretically. The dominant electron transfer pathway is elucidated via DFT in this work. As observed from the charge density difference results (Fig. 7b), with localized unpaired electrons, doping with could be considered efficient in adjusting the spin density and charge distribution of inert carbonaceous materials [22]. According to the calculation result of charge density difference distribution (Fig. 7a and b), the existence of N on the pure N-doped carbon materials results in certain electron transfer with PI. Besides, the calculated adsorption energy between PI and N was 3.09 eV, suggesting a relatively weak physical absorption of IO_4^- on N atoms. This confirms the hypothesis detailed above (that N could work as a reactive site during the activation of PI). However, unlike pure N-doped carbon material, pure Fe-doped carbon material exhibited chemisorption between Fe and IO_4^- via a "donor-acceptor complex" mechanism [57], forming a strong Fe–O covalent bond with a bond length of 1.86 Å (Fig. 7d). Moreover, the Fe, N co-doping system exhibited more superior performance than pure N- or Fe-doped carbonaceous materials. On the one hand, when Fe and N are co-doped in carbon materials, Fe–O's bond length is reduced to 1.82 Å (Fig. 7f), indicating a more stable chemical bond. This also explains the higher adsorption energy of the Fe, N co-doped system with PI (6.82 eV), compared with that of pure Fe-doped (6.69 eV) and pure N-doped systems (3.09 eV) (Fig. 7a, c, and e). On the other hand, as observed from the charge density difference results of the CWBC/PI system (Fig. 7f), an electron transfer channel between CWBC and PI was established, further confirming the powerful electron transfer mechanism that existed in the degradation of SDZ. As a result, the I–O bond on the Fe, N co-doped CWBC material can be prolonged to 1.93 Å, compared with pure Fe-doped (1.89 Å) and N-doped (1.79 Å) carbonaceous material. The

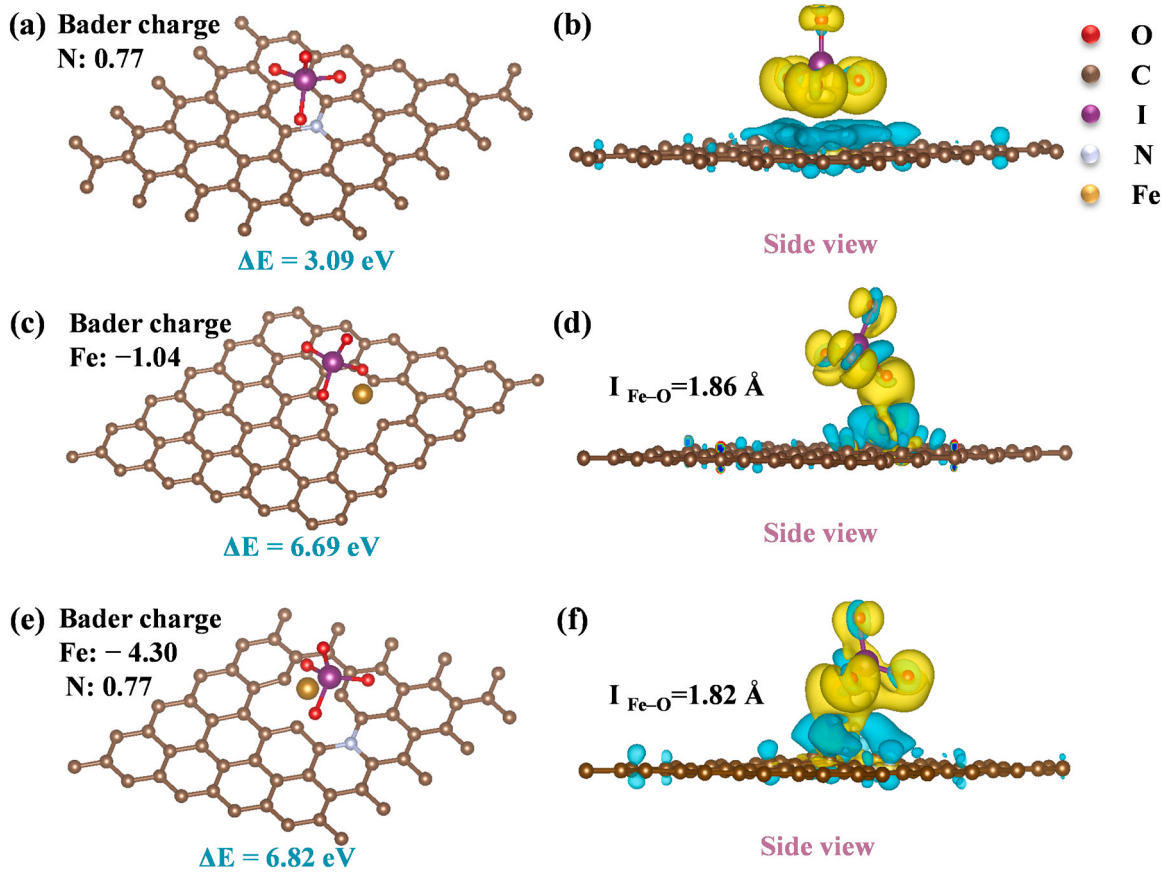

Fig. 7. Optimized adsorption model for IO_4^- species on the surface of pure N doped carbon (a), pure Fe doped carbon (c), and Fe, N co-doped carbon (CWBC) (e); Sideview of charge density difference distribution of IO_4^- on (b) pure N doped, (d) pure Fe doped, and (f) Fe, N co-doped carbon surface. The yellow areas denote the accumulation of electrons while the turquoise areas represent the depletion of electrons.

prolonged bond length of the I—O bond means that PI is more likely to decompose. Thus, an electron transfer process could be improved.

In conclusion, the primary function of N, with a positive Bader charge, is to facilitate the rearrangement of the charge distribution and breakage of the inert carbon matrix when it is co-doped with Fe. After introducing N, the Fe–O covalent bond is more stable, and the adsorption energy between CWBC and PI is higher than without N. In addition, according to the result of XPS investigations, N could also work as an adsorption sites and electron transfer mediator, as discussed before. However, this function is relatively negligible in this co-doped material. In contrast, Fe mainly functions as an active site for electron transfer in the co-doped system. In the presence of N atoms, the electron loss capacity of Fe can be enhanced with a Bader charge value from − 1.04 to − 4.30 (Fig. 7c and e), fastening the electron transfer process. Simultaneously, electron-deficient C regions are formed on the surface of the carbon matrix of CWBC due to the withdrawing of electrons by N and Fe. As a result, SDZ with electron-donating groups as an electron donor will replace to balance the loss of the electrons in the carbonaceous matrix, forming an electron cycle.

Therefore, an electron channel was formed among SDZ, CWBC, and PI. The electrons were dragged from the pollutant to the electron-withdrawing Fe center and then straightway provided to PI for decomposing. A closed circuit of electrons maintains the equilibrium between the gain and loss of electrons in the system, ensuring an efficient SDZ degradation by CWBC activated PI reactions. The slight decrease in activity with increasing recycles could be due to the inevitable reduction of some catalytic sites and the leaching of traces of iron on the catalyst [58]. Based on the above analysis, an electron-transfer dominated mechanism in the CWBC/PI system for SDZ removal is described as follows (Eq. (21)):

$$SDZ + \left[C\xrightarrow{\overrightarrow{e}^{N}_{Fe}} \widehat{CWBC} \right] \overbrace{\overrightarrow{e} - IO_4^- \left] \xrightarrow{\overrightarrow{e}^{Fe-}_{O}} \right.}^{C\xrightarrow{\overrightarrow{e}^{N}_{Fe}}} SDZ_{products} + CWBC + IO_3^- \quad (21)$$

Therein, $\widehat{CWBC}$ stand for the inner electron transfer of CWBC.

During this reaction, the transformation of PI after activation by CWBC was measured. As shown in Fig. S5, more than 95% of the decomposed IO_4^- converted to IO_3^- product, which is nontoxic and a safe sink of iodine species for iodinated byproducts production [2]. Similar phenomenon has been reported by Long et al. [59], who confirmed the stoichiometrically converted of PI to IO_3^- when degrade organic pollutant in the system of Co active sites supported by N-doped graphene/PI. Correspondingly, the amount of I^- and other iodine species transformed from the utilized part of PI were little (< 4.5%), indicating further transformation of IO_3^- to I^- and I_2 hardly happen. In conclusion, the test of PI transformation confirms the electron-transfer dominated mechanism proposed in Eq. (21), that IO_4^- could convert to IO_3^- after the reaction.

3.6. Degradation products and pathways

The degradation intermediates formed by the removal of SDZ were detected by QTOF LC/MS. Seven possible degradation products were identified with *m/z* peaks of 82.0388, 94.0657, 95.0483, 114.0162,

118.0816, 187.0984, and 217.0718. Based on these identified intermediates, two plausible degradation pathways are summarized in Fig. 8 and Table S4. First, cleavage of the S—N bond is confirmed by the formation of 2-aminopyrimidine (B1). Therefore, the detected 2H-imidazol-2-imine (B2) is possibly assigned to degradation of B1 further. Second, the presence of 4-[2-imino-pyrimidine-l(2H)-yl] aniline (C1) shows that SO_2 extrusion happens during the degradation reaction. This is a frequently reported pathway for SDZ degradation by AOP processes. During this process, the $–NH_2$ groups on C1 can be oxidized by direct electron transfer and radical attack [40], forming C2. Simultaneously, the C–N bond of C1 is easily broken under the further attack of $O_2^{\bullet-}$, producing aniline. The intermediate products are further decomposed into ring-opening products such as 5-amino valeric acid (C4) and α-hydroxyglycine (B3). The detection of these small molecules products indicates the strong mineralization capability by CWBC/PI oxidation.

4. Implication

We report herein a waste-treat-waste mode for simultaneous persistent organic compounds removal and hazardous solid waste disposal. The CWBC-activated PI-based AOPs exhibited several remarkable merits that were ideally suited for wastewater treatment applications. First, PI/CWBC system does not need extra energy input, unlike UV irradiation, electricity, and ultrasound activation. Second, the system exhibited excellent degradation reactivity under anoxic conditions. This result suggests that the developed PI/CWBC process has an appealing potential when combined with the biotreatment technologies, especially for anaerobic biological treatment. Additionally, this PI/CWBC system could deal with emergencies that the contaminants need to be removed because PI is activated rapidly [2]. Worthwhile, the system presents a promising oxidation technology for treating of various pollutants that contain heterocyclic groups, azo benzene, carboxyl, and aniline because of the fast and efficient removal of pollutants. The removal of a series of organic pollutants, including antibiotics (CTC, SMX, NOR), nonsteroidal anti-inflammatory drugs (IBU, DCF), endocrine-disrupting chemical (BPA), and dye (RR2) (40 μM), was investigated by the present PI/CWBC system. As seen in Fig. S6, about 100% of CTC, 66.12% of SMX, 77.20% of NOR, 72.46% of IBU, 95.63% of DCF, 98.91% of BPA, and 92.08% of RR2 were removed within 90 min when the PI/CWBC system was applied.

This work guides designing inexpensive and high-performance PI activators inspired by the coagulation waste from the paper mill industry. Similarly, solid waste containing lignocellulose components and transition metals, such as CW from traditional Chinese medicine, could all be prepared to the activators via the facile preparation method. Compared with other AOPs oxidants like PMS, this system has several advantages: (1) The PI/CWBC system can be used for specific application scenarios where PMS are not suitable. (2) In this study, this system also showed a promoting effect on SDZ degradation under anoxic conditions. Enhanced degradation efficiency of SDZ was achieved under N_2 purging during the reaction process. However, future studies, including the mechanism analyses and durability tests, are still needed for further application. The reaction kinetics and activation pathway of PI activation under anoxic conditions may be further understood by experimental study. Moreover, further research is needed to explore the effect of heteroatoms doped catalysts on PI activation.

5. Conclusion

In summary, we have demonstrated a CW-based Fe, N co-doped catalyst with superior performance to active PI for antibiotic degradation. Under appropriate conditions, 98.94% of SDZ was removed within a reaction of 90 min. Radicals ($O_2^{\bullet-}$, RIS, and PFRs) and non-radical (electron transfer) pathways were confirmed to contribute to SDZ degradation, whereas the latter was found as the predominant pathway. The DFT calculations showed that the co-doping of Fe and N induced electronic structure modulation, strengthening the electron loss capacity of Fe to the chemisorbed IO_4^- via Fe–O covalent bond. The strong covalent linkage between Fe species and IO_4^- can prolong the I–O bond and boost IO_4^- decomposition, thus enhancing the electron transfer pathway. Meanwhile, electrons on SDZ were dragged to the CWBC to maintain electronic balance, ensuring the continuous efficiency of SDZ degradation. Two degradation pathways, including cleavage of the S—N bond and SO_2 extrusion, were deduced during the degradation process. This work opens up a new perspective for cost-effective lignocellulose-containing waste recycle and broadens out the avenue for PI-based AOPs in the treatment of refractory organic micropollutants.

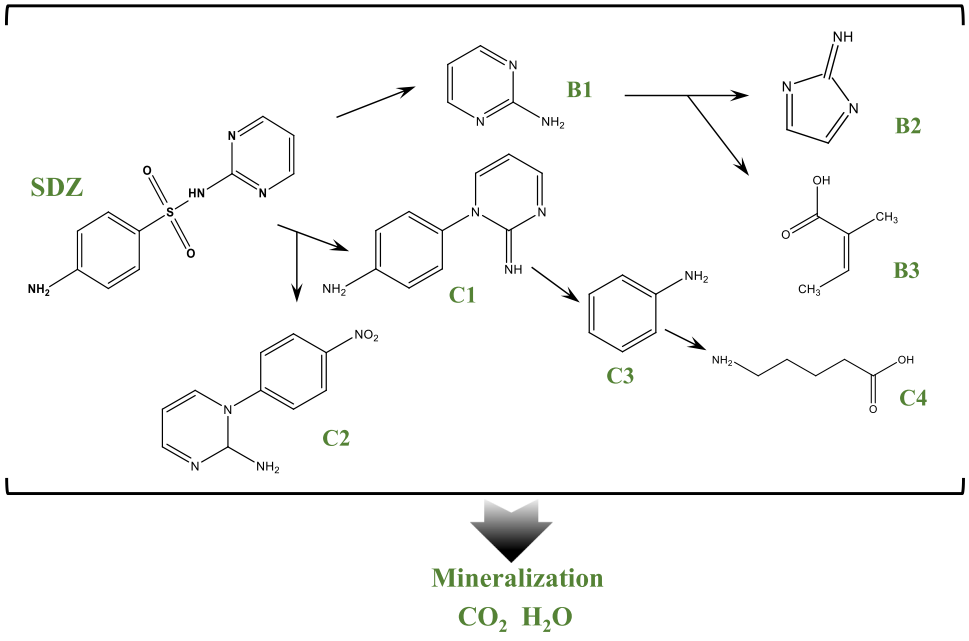

Fig. 8. Proposed pathways for SDZ degradation during CWBC–PI oxidation. Compounds with capital letters were detected by QTOF LC/MS.

CRediT authorship contribution statement

Lei He: Conceptualization, Methodology, Data curation, Supervision, Writing – original draft. **Chao Yang:** Sample collection and analysis, Drawing, Investigation. **Jie Ding:** Supervision, Validation, Writing – review & editing, Funding acquisition. **Mei-Yun Lu:** Sample collection and analysis, Investigation. **Cheng-Xin Chen:** Methodology. **Guang-Yuan Wang:** Writing – review & editing. **Jun-Qiu Jiang:** Methodology. **Lan Ding:** Sample collection and analysis. **Guo-Shuai Liu:** Formal analysis, writing – review & editing. **Nan-Qi Ren:** Conceptualization-experimental design. **Shan-Shan Yang:** Conceptualization, Supervision, Validation, Writing – review & editing.

Declaration of Competing Interest

The authors declare that they have no known competing financial interests or personal relationships that could have appeared to influence the work reported in this paper.

Acknowledgements

The authors gratefully acknowledge the National Natural Science Foundation of China, China (Grant No. 52170131); the State Key Laboratory of Urban Water Resource and Environment (Harbin Institute of Technology, China) (Grant No. 2021TS03); the Research and Application of Treatment Technology for High Concentration and Refractory Wastewater (Printing and Dyeing, Pharmaceutical, Chemical), China (GJSZ2021030907-YF). We gratefully acknowledge supports of Heilongjiang Province Touyan Team.

Appendix A. Supporting information

Supplementary data associated with this article can be found in the online version at doi:10.1016/j.apcatb.2021.120880.

References

[1] H.W. Luo, Y.F. Zeng, D.Q. He, X.L. Pan, Application of iron-based materials in heterogeneous advanced oxidation processes for wastewater treatment: a review, Chem. Eng. J. 407 (2021), 127191.
[2] H.W. Sun, F. He, W.Y. Choi, Production of reactive oxygen species by the reaction of periodate and hydroxylamine for rapid removal of organic pollutants and waterborne bacteria, Environ. Sci. Technol. 54 (2020) 6427–6437.
[3] Y. Zong, Y.F. Shao, Y.Q. Zeng, B.B. Shao, L.Q. Xu, Z.Y. Zhao, W. Liu, D.L. Wu, Enhanced oxidation of organic contaminants by iron(II)-activated periodate: the significance of high-valent iron-oxo species, Environ. Sci. Technol. 55 (2021) 7634–7642.
[4] H. Lee, H.Y. Yoo, J. Choi, I.H. Nam, S. Lee, S. Lee, J.H. Kim, C. Lee, J. Lee, Oxidizing capacity of periodate activated with iron-based bimetallic nanoparticles, Environ. Sci. Technol. 48 (2014) 8086–8093.
[5] L.Y. He, L.X. Lv, S.C. Pillai, H.L. Wang, J.M. Xue, Y.F. Ma, Y.L. Liu, Y.L. Chen, L. Wu, Z.L. Zhang, L. Yang, Efficient degradation of diclofenac sodium by periodate activation using Fe/Cu bimetallic modified sewage sludge biochar/UV system, Sci. Total Environ. 783 (2021), 146974.
[6] Q. Wang, H. Zeng, Y.H. Liang, Y. Cao, Y. Xiao, J. Ma, Degradation of bisphenol AF in water by periodate activation with FeS (mackinawite) and the role of sulfur species in the generation of sulfate radicals, Chem. Eng. J. 407 (2021), 126738.
[7] Y. Choi, H.I. Yoon, C. Lee, L. Vetrakova, D. Heger, K. Kim, J. Kim, Activation of periodate by freezing for the degradation of aqueous organic pollutants, Environ. Sci. Technol. 52 (2018) 5378–5385.
[8] Y.C. Lee, M.J. Chen, C.P. Huang, J. Kuo, S.L. Lo, Efficient sonochemical degradation of perfluorooctanoic acid using periodate, Ultrason. Sonochem. 31 (2016) 499–505.
[9] A.D. Bokare, W. Choi, Singlet-oxygen generation in alkaline periodate solution, Environ. Sci. Technol. 49 (2015) 14392–14400.
[10] L.H. Chia, X.M. Tang, L.K. Weavers, Kinetics and mechanism of photoactivated periodate reaction with 4-chlorophenol in acidic solution, Environ. Sci. Technol. 38 (2004) 6875–6880.
[11] E.T. Yun, H.Y. Yoo, W. Kim, H.E. Kim, G. Kang, H. Lee, S. Lee, T. Park, C. Lee, J. H. Kim, J. Lee, Visible-light-induced activation of periodate that mimics dye-sensitization of TiO_2: simultaneous decolorization of dyes and production of oxidizing radicals, Appl. Catal. B: Environ. 203 (2017) 475–484.
[12] A. Haddad, S. Merouani, C. Hannachi, O. Hamdaoui, B. Hamrouni, Intensification of light green SF yellowish (LGSFY) photodegradion in water by iodate ions: iodine radicals implication in the degradation process and impacts of water matrix components, Sci. Total Environ. 652 (2019) 1219–1227.
[13] J.K. Du, S.G. Tang, H.B. Faheem, H. Ling, G.F. Zheng, L.T. Xiao, J.G. Luo, Bao, Insights into periodate oxidation of bisphenol A mediated by manganese, Chem. Eng. J. 369 (2019) 1034–1039.
[14] H.Z. Wang, W.Q. Guo, B.H. Liu, Q.L. Wu, H.C. Luo, Q. Zhao, Q.S. Si, F. Sseguya, N. Q. Ren, Edge-nitrogenated biochar for efficient peroxydisulfate activation: an electron transfer mechanism, Water Res. 160 (2019) 405–414.
[15] H.C. Zhang, J.J. Han, X. Zhang, P.C. Guo, D.H. Xie, G.P. Sheng, Undiscovered multiple roles of multivalent cations in the pollutant removal from actual water by persulfate activated by carbon materials, ACS EST Eng. (2021), 1c00121.
[16] X.W. Li, X.T. Liu, C.D. Qi, C.Y. Lin, Activation of periodate by granular activated carbon for acid orange 7 decolorization, J. Taiwan Inst. Chem. Eng. 68 (2016) 211–217.
[17] L.J. Peng, Y.N. Shang, B.Y. Gao, X. Xu, Co3O4 anchored in N, S heteroatom co-doped porous carbons for degradation of organic contaminant: role of pyridinic N-Co binding and high tolerance of chloride, Appl. Catal. B: Environ. 282 (2021), 119484.
[18] X. Li, Y. Jia, H.M. Zhou, X.F. Su, J.H. Sun, High-efficiency degradation of organic pollutants with Fe, N co-doped biochar catalysts via persulfate activation, J. Hazard. Mater. 397 (2020), 122764.
[19] X.G. Duan, H.Q. Sun, Y.X. Wang, J. Kang, S.B. Wang, N-doping-induced nonradical reaction on single-walled carbon nanotubes for catalytic phenol oxidation, ACS Catal. 5 (2015) 553–559.
[20] D.H. Ding, S.J. Yang, X.Y. Qian, L.W. Chen, T.M. Cai, Nitrogen-doping positively whilst sulfur-doping negatively affect the catalytic activity of biochar for the degradation of organic contaminant, Appl. Catal. B: Environ. 263 (2020), 118348.
[21] W.Q. Tian, Q.M. Gao, A. VahidMohammadi, J. Dang, Z.Y. Li, X. Liang, M. M. Hamedi, L.M. Zhang, Liquid-phase exfoliation of layered biochars into multifunctional heteroatom (Fe, N, S) co-doped graphene-like carbon nanosheets, Chem. Eng. J. 420 (2021), 127601.
[22] S.J. Ye, G.M. Zeng, X.F. Tan, H.P. Wu, J. Liang, B. Song, N. Tang, P. Zhang, Y. Y. Yang, Q. Chen, X.P. Li, Nitrogen-doped biochar fiber with graphitization from Boehmeria nivea for promoted peroxymonosulfate activation and non-radical degradation pathways with enhancing electron transfer, Appl. Catal. B: Environ. 269 (2020), 118850.
[23] L. Peng, X.G. Duan, Y.N. Shang, B.Y. Gao, X. Xu, Engineered carbon supported single iron atom sites and iron clusters from Fe-rich Enteromorpha for Fenton-like reactions via nonradical pathways, Appl. Catal. B: Environ. 287 (2021), 119963.
[24] S.J. Yu, J.Z. Sun, Y.F. Shi, Q.Q. Wang, J. Wu, J. Liu, Nanocellulose from various biomass wastes: its preparation and potential usages towards the high value-added products, Environ. Sci. Ecotechnol. 5 (2021), 100077.
[25] S. Yang, W. Li, H.J. Zhang, Y.B. Wen, Y.H. Ni, Treatment of paper mill wastewater using a composite inorganic coagulant prepared from steel mill waste pickling liquor, Sep. Purif. Technol. 209 (2019) 238–245.
[26] M.S. Hossain, F. Omar, A.J. Asis, R.T. Bachmann, M.Z.I. Sarker, M.O. Ab Kadir, Effective treatment of palm oil mill effluent using $FeSO_4{\cdot}7H_2O$ waste from titanium oxide industry: coagulation adsorption isotherm and kinetics studies, J. Clean. Prod. 219 (2019) 86–98.
[27] A. Khan, M. Mirza, B. Fa Hlman, R. Rybchuk, J. Yang, D. Harfield, A.O. Anyia, Mapping thermomechanical pulp sludge (TMPS) biochar characteristics for greenhouse produce safety, J. Agric. Food Chem. 63 (2015) 1648–1657.
[28] M.M. Manyuchi, N. Chaukura, C. Ruzvidzo, Techno-economic assessment for biochar production from paper mill sludge, Research and Intellectual Outputs 2016-Science, Engineering and Technology, 30 August–4 September 2016, NUST Bulawayo, 5, 2016.
[29] J.K. Du, G.F. Xiao, Y.X. Xi, X.W. Zhu, F. Su, S.H. Kim, Periodate activation with manganese oxides for sulfanilamide degradation, Water Res. 169 (2020), 115278.
[30] Q.C. Zhang, Z.J. Du, X.Z. Huang, Z.X. Zhao, T. Guo, G.T. Zeng, Y.T. Yu, Tunable microwave absorptivity in reduced graphene oxide functionalized with Fe_3O_4 nanorods, Appl. Surf. Sci. 473 (2019) 706–714.
[31] J.F. Yu, L. Tang, Y. Pang, G.M. Zeng, H.P. Feng, J.J. Zou, J.J. Wang, C.Y. Feng, X. Zhu, X.L. Ouyang, J.S. Tan, Hierarchical porous biochar from shrimp shell for persulfate activation: a two-electron transfer path and key impact factors, Appl. Catal. B: Environ. 260 (2020), 118160.
[32] J.X. Zhong, H. Jiang, Z.L. Wang, Z.G. Yu, L.Z. Wang, J.F. Mueller, J.H. Guo, Efficient photocatalytic destruction of recalcitrant micropollutants using graphitic carbon nitride under simulated sunlight irradiation, Environ. Sci. Ecotechnol. 5 (2021), 100079.
[33] K. Zhu, Q. Bin, Y. Shen, J. Huang, D. He, W. Chen, In-situ formed N-doped bamboo-like carbon nanotubes encapsulated with Fe nanoparticles supported by biochar as highly efficient catalyst for activation of PS toward degradation of organic pollutants, Chem. Eng. J. 402 (2020), 126090.
[34] L. Xu, B. Fu, Y. Sun, P. Jin, X. Bai, X. Jin, X. Shi, Y. Wang, S. Nie, Degradation of organic pollutants by Fe/N co-doped biochar via peroxymonosulfate activation: synthesis, performance, mechanism and its potential for practical application, Chem. Eng. J. 400 (2020), 125870.
[35] Z.Y. Zhang, X.Y. Huang, J. Ma, Z.G. Pei, Efficient removal of bisphenol S by non-radical activation of peroxydisulfate in the presence of nano-graphite, Water Res. 8 (2021), 117288.
[36] A. Shan, A. Idrees, W.Q. Zaman, Z. Abbas, U. Farooq, M. Ali, R. Yang, G.L. Zeng, M. Danish, X.G. Gu, S.G. Lyu, Enhancement in reactivity via sulfidation of FeNi@BC for efficient removal of trichloroethylene: insight mechanism and the role of reactive oxygen species, Sci. Total Environ. 794 (2021), 148674.
[37] X.X. Huang, N.W. Zhu, X.R. Wei, Y. Ding, Y.X. Ke, P.X. Wu, Z.H. Liu, Mechanism insight into efficient peroxydisulfate activation by novel nano zero-valent iron

anchored yCo_3O_4 (nZVI/yCo_3O_4) composites, J. Hazard. Mater. 400 (2020), 123157.
[38] D. Ouyang, Y. Chen, J.C. Yan, L.B. Qian, L. Han, M.F. Chen, Activation mechanism of peroxymonosulfate by biochar for catalytic degradation of 1,4-dioxane: important role of biochar defect structures, Chem. Eng. J. 370 (2019) 614–624.
[39] C. Lee, J. Yoon, Application of photoactivated periodate to the decolorization of reactive dye: reaction parameters and mechanism, J. Photoch. Photobiol. A 165 (2004) 35–41.
[40] W.Q. Guo, Q. Zhao, J.S. Du, H.Z. Wang, X.F. Li, N.Q. Ren, Enhanced removal of sulfadiazine by sulfidated ZVI activated persulfate process: performance, mechanisms and degradation pathways, Chem. Eng. J. 388 (2020), 124303.
[41] J.K. Du, G.F. Xiao, Y.X. Xi, X.W. Zhu, F. Su, S.H. Kim, Periodate activation with manganese oxides for sulfanilamide degradation, Water Res. 169 (2020), 115278.
[42] C. Guillard, E. Puzenat, H. Lachheb, A. Houas, J.M. Herrmann, Why inorganic salts decrease the TiO_2 photocatalytic efficiency, J. Alloy. Compd. 503 (2007) 485–489.
[43] C.X. Chen, S.S. Yang, J. Ding, G.Y. Wang, L. Zhong, S.Y. Zhao, Y.N. Zang, J. Q. Jiang, L. Ding, Y. Zhao, L.M. Liu, N.Q. Ren, Non-covalent self-assembly synthesis of AQ2S@rGO nanocomposite for the degradation of sulfadiazine under solar irradiation: the indispensable effect of chloride, Appl. Catal. B: Environ. 298 (2021), 120495.
[44] H. Li, Y.F. Qiu, X.L. Wang, J. Yang, Y.J. Yu, Y.Q. Chen, Y.D. Liu, Biochar supported Ni/Fe bimetallic nanoparticles to remove 1,1,1-trichloroethane under various reaction conditions, Chemosphere 169 (2017) 534–541.
[45] Y.F. Qi, J. Li, Y.Q. Zhang, Q. Cao, Y.M. Si, Z.R. Wu, M. Akram, X. Xu, Novel lignin-based single atom catalysts as peroxymonosulfate activator for pollutants degradation: role of single cobalt and electron transfer pathway, Appl. Catal. B: Environ. 286 (2021), 119910.
[46] S.S. Zhu, C. Jin, X.G. Duan, S.B. Wang, S.H. Ho, Nonradical oxidation in persulfate activation by graphene-like nanosheets (GNS): differentiating the contributions of singlet oxygen ($^1O_2$) and sorption-dependent electron transfer, Chem. Eng. J. 393 (2020), 124725.
[47] Y.X. Guo, L.G. Yan, X.G. Li, T. Yan, W. Song, T.L. Hou, C.L. Tong, J.L. Mu, M. Xu, Goethite/biochar-activated peroxymonosulfate enhances tetracycline degradation: inherent roles of radical and non-radical processes, Sci. Total Environ. 783 (2021), 147102.
[48] L. Meunier, H. Laubscher, S.J. Hug, B. Sulzberger, Effects of size and origin of natural dissolved organic matter compounds on the redox cycling of iron in sunlit surface waters, Aquat. Sci. 67 (2005) 292–307.
[49] J. Brame, M. Long, Q. Li, P. Alvarez, Trading oxidation power for efficiency: differential inhibition of photo-generated hydroxyl radicals versus singlet oxygen, Water Res. 60 (2014) 259–266.
[50] Y.D. Chen, X. Duan, C. Zhang, S. Wang, N.Q. Ren, S.H. Ho, Graphitic biochar catalysts from anaerobic digestion sludge for nonradical degradation of micropollutants and disinfection, Chem. Eng. J. 384 (2020), 123244.
[51] Y. Guo, L. Yan, X. Li, T. Yan, W. Song, T. Hou, C. Tong, J. Mu, M. Xu, Goethite/biochar-activated peroxymonosulfate enhances tetracycline degradation: inherent roles of radical and non-radical processes, Sci. Total Environ. 783 (2021), 147102.
[52] J. Yang, B. Pan, H. Li, S.H. Liao, D. Zhang, M. Wu, B.S. Xing, Degradation of p-nitrophenol on biochars: role of persistent free radicals, Environ. Sci. Technol. 50 (2016) 694–700.
[53] G.D. Fang, C. Liu, J. Gao, D.D. Dionysiou, D.M. Zhou, Manipulation of persistent free radicals in biochar to activate persulfate for contaminant degradation, Environ. Sci. Technol. 49 (2015) 5645–5653.
[54] H.Z. Wang, W.Q. Guo, R.L. Yin, J.S. Du, Q.L. Wu, H.C. Luo, B.H. Liu, F. Sseguya, N. Q. Ren, Biochar-induced Fe(III) reduction for persulfate activation in sulfamethoxazole degradation: insight into the electron transfer, radical oxidation and degradation pathways, Chem. Eng. J. 362 (2019) 561–569.
[55] E.T. Yun, J.H. Lee, J. Kim, H.D. Park, J. Lee, Identifying the nonradical mechanism in the peroxymonosulfate activation process: singlet oxygenation versus mediated electron transfer, Environ. Sci. Technol. 52 (2018) 7032–7042.
[56] J.W. Pan, B.Y. Gao, P.J. Duan, K.Y. Guo, M. Akram, X. Xu, Q.Y. Yue, Y. Gao, Improving peroxymonosulfate activation by copper ion-saturated adsorbent-based single atom catalysts for the degradation of organic contaminants: electron-transfer mechanism and the key role of Cu single atoms, J. Mater. Chem. A 19 (2021) 11604–11613.
[57] A. Dąbrowski, P. Podkościelny, Z. Hubicki, M. Barczak, Adsorption of phenoliccompounds by activated carbon-a critical review, Chemosphere 58 (2005) 1049–1070.
[58] X. Zhang, Z.P. Yao, Y. Zhou, Z.R. Zhang, G.F. Lu, Z.H. Jiang, Theoretical guidance for the construction of electron-rich reaction microcenters on C-O-Fe bridges for enhanced Fenton-like degradation of tetracycline hydrochloride, Chem. Eng. J. 411 (2021), 128535.
[59] Y. Long, J. Dai, S. Zhao, Y. Su, Z. Wang, Z. Zhang, Atomically dispersed cobalt sites on graphene as efficient periodate activators for selective organic pollutant degradation, Environ. Sci. Technol. 55 (2021) 5357–5370.